Submitted Manuscript

Applied Spectroscopy

www.s-a-s.org

Raman Spectroscopic Detection and Quantification of Macro- and Microhematuria in Human Urine

Applied Spectroscopy
2022, Vol. 0(0) 1–11

DOI: 10.1177/00037028211060853
journals.sagepub.com/home/asp
SAGE

William Carswell[1], John L. Robertson[2,3], and Ryan S. Senger[1,3,4,5]

Abstract

Hematuria refers to the presence of blood in urine. Even in small amounts, it may be indicative of disease, ranging from urinary tract infection to cancer. Here, Raman spectroscopy was used to detect and quantify macro- and microhematuria in human urine samples. Anticoagulated whole blood was mixed with freshly collected urine to achieve concentrations of 0, 0.25, 0.5, 1, 2, 6, 10, and 20% blood/urine (v/v). Raman spectra were obtained at 785 nm and data analyzed using chemometric methods and statistical tests with the Rametrix toolboxes for Matlab. Goldindec and iterative smoothing splines with root error adjustment (ISREA) baselining algorithms were used in processing and normalization of Raman spectra. Rametrix was used to apply principal component analysis (PCA), develop discriminate analysis of principal component (DAPC) models, and to validate these models using external leave-one-out cross-validation (LOOCV). Discriminate analysis of principal component models were capable of detecting various levels of microhematuria in unknown urine samples, with prediction accuracies of 91% (using Goldindec spectral baselining) and 94% (using ISREA baselining). Partial least squares regression (PLSR) was then used to estimate/quantify the amount of blood (v/v) in a urine sample, based on its Raman spectrum. Comparing actual and predicted (from Raman spectral computations) hematuria levels, a coefficient of determination (R^2) of 0.91 was obtained over all hematuria levels (0–20% v/v), and an R^2 of 0.92 was obtained for microhematuria (0–1% v/v) specifically. Overall, the results of this preliminary study suggest that Raman spectroscopy and chemometric analyses can be used to detect and quantify macro- and microhematuria in unprocessed, clinically relevant urine specimens.

Keywords

Hematuria, urinalysis, Raman spectroscopy, bladder cancer, chemometric analysis, macrohematuria, microhematuria, human urine

Date received: 18 December 2020; accepted: 25 May 2021

Introduction

The presence of blood in urine is abnormal and is frequently associated with disease in the genitourinary tract (kidneys, bladder, and male/female reproductive organs). The presence of blood in urine ("hematuria") may be suspected by obvious red-brown discoloration of urine (macrohematuria). Small amounts of blood (microhematuria) may not discolor urine or be detected visually, but discovered with urinalysis in patients displaying clinical signs of genitourinary disease. Detection or suspicion of hematuria is invariably confirmed with other medical tests, including urine sediment examination, biochemical (dry chemistry, "dipstick") assays, and multimodality imaging.[1–4]

Hematuria can be caused by a large variety of diseases (ranging, e.g., from bladder infections to cancer), injuries, or even exposure to toxicants (such as the chemotherapeutic agent cyclophosphamide).[2,5,6] Testing for macrohematuria and early intervention has been shown to be cost effective,[7] but early, aggressive testing for microhematuria has not been

[1]Department of Biological Systems Engineering, Virginia Tech, Blacksburg, Virginia, USA
[2]Department of Biomedical Engineering and Mechanics, Virginia Tech, Blacksburg, Virginia, USA
[3]DialySensors, Inc., Blacksburg, Virginia, USA
[4]Department of Chemical Engineering, Virginia Tech, Blacksburg, Virginia, USA
[5]Department of Surgery, Virginia Commonwealth University, Richmond, Virginia, USA

Corresponding author:
Ryan S. Senger, Department of Biological Systems Engineering, Virginia Tech, 1230 Washington St. SW, Blacksburg, VA 24061, USA.
Email: senger@vt.edu

shown to produce an increased health benefit (i.e., early detection of disease) compared to the cost of screening at-risk populations.[8] Laboratory costs and technician time associated with testing for hematuria make generalized population screening logistically and economically impractical. Here, we present a low cost, low impact screening method for detecting both macro- and microhematuria that relies on evaluation of urine using Raman spectroscopy and chemometric methods implemented with Rametrix software.[9–14]

Raman spectroscopy is a well-documented spectrographic method of examining the molecular composition of both solids and solutions.[3,9,13,15,16] When examining even dilute and complex aqueous solutions (such as urine),[3,9–13,15–20] Raman spectroscopy may take on the order of seconds to generate spectral data, with minimal spectral interference from water. Analysis of aqueous solution spectra involves data transformation in the form of baseline correction, truncation, normalization, and statistical processing. These transformations help to eliminate various spectral artifacts such as autofluorescence, photobleaching, cosmic spikes, and background signals. Two baselining methods used in this study were the Goldindec[21] and iterative smoothing-splines with root error adjustment (ISREA) methods.[22] The Goldindec algorithm provides an adaptable means to subtract background signals and baseline Raman spectra.[10,14,23] The recently developed ISREA method has been optimized for full baseline fitting, even at the ends of spectra.[22] The ISREA method uses cubic splines to connect knots (or "nodes") placed at specific Raman shifts throughout a spectrum. This has shown to allow optimization of data analysis for presumed target molecules, and it may provide modeling advantages by removing interference from other, unrelated spectral data.[22]

Principal component analysis (PCA) and discriminant analysis of principal components (DAPC) are multivariate statistical analysis methods for complex datasets. Previously, we reported that these methods are useful in assessing the qualitative similarity and difference between spectra.[9,12,13] In particular, PCA is an unsupervised method that serves to reduce data-rich spectra from hundreds of intensity values into a small number (e.g., 5–30) of principal components (PCs). Discriminate analysis of principal components, on the other hand, is a supervised algorithm that maps PCs to some characteristic of the sample (e.g., levels of hematuria). This procedure is subject to validation, and leave-one-out cross-validation (LOOCV) has been used in several studies. With these results, metrics such as overall accuracy, sensitivity, specificity, positive predictive value (PPV), and negative predictive value (NPV) are calculated. From there, PCA and DAPC loadings represent Raman shifts that distinguish groups of spectra from one another. These are traced to individual molecules (using Raman shift databases) that are involved in the disease pathology (e.g., heme associated with hematuria).[10–12]

In addition to these chemometric methods, more direct comparisons of spectra have been used to determine if statistically significant differences exist. One approach is to calculate the total principal component distance (TPD) between two Raman spectra. With urine, this involves finding the difference between each PC of a urine spectrum and the corresponding PC of a control. This control can be the average spectrum of a stable chemical or formulation (e.g., the urinalysis control Surine), or it could be the average spectrum of a sample at an initial time point. The TPD is then calculated by summing the absolute values of these differences between PCs.[10,11,14] Once TPD values are determined, statistical tests, including analysis of variance (ANOVA) and pairwise comparisons, are applied to these values to determine if/where statistically significant differences exist between groups of spectra. In the context of analyzing urine specimens, this approach has been used to determine if Raman spectra of urine from healthy volunteers are statistically different from those of patients with chronic kidney disease.[11]

Evaluating hematuria quantitatively is an important goal of urinalysis, as the amount of blood in urine can be an important diagnostic metric when determining cause, severity, and etiology of the hematuria.[1,6,8] We believe that generating a calibration curve is critical when using Raman spectroscopy to define quantitative values, but in cases where the molecular signature of the molecule or solution is complex, creating meaningful calibration curves and standards can be complex or ineffective.[13] To address this complexity, partial least squares regression (PLSR) can be useful in evaluating complex datasets and correlating those datasets to quantitative classifications.[24] This approach was used here, in place of a calibration curve, and used to generate a model that can predict the amount of blood in a urine sample given its Raman spectrum.

For this study, we hypothesized that both macro- and microhematuria could be detected and quantified from Raman spectral analysis of human urine and chemometric analyses. Specifically, we sought to determine: (i) Are Raman spectra of urine "spiked" with whole blood (i.e., a model of hematuria) statistically different from those without the addition of blood (i.e., no hematuria); (ii) can the presence of large amounts of spiked blood (i.e., a model of macrohematuria) be distinguished from small amounts of spiked blood (i.e., a model of microhematuria); and (iii) can the quantity of spiked blood (i.e., the degree of hematuria) be quantified.

Materials and Methods

Informed Consent and Urine Specimen Collection

Informed written consent was obtained for the collection of specimens from healthy volunteers affiliated with Virginia Tech, under an institutional review board-approved protocol (VT-IRB 15-703). The hematuria dataset was composed of urine specimens generated to simulate macro- and microhematuria of varying levels of severity. In particular, urine and blood were collected the same day from an

informed, healthy volunteer. The urine specimen was screened for hematuria using Multistix 10 SG urinalysis test strips (Siemens, USA).

Hematuria Samples and Surine

Once confirmed the urine was free of blood, the "macrohematuria" samples were generated by mixing a 20% v/v solution (4 mL urine with 1 mL of blood), then diluting with urine to produce 10% and 6% volume of blood samples. "Microhematuria" samples were generated by initially mixing a 2% v/v solution (49 mL of urine with 1 mL of blood). Then, 1, 0.5, and 0.25% mixtures were obtained through dilutions with urine. The resulting hematuria dataset contained urine samples with no blood (0% v/v), microhematuria (0.25, 0.5, and 1%), and macrohematuria (2, 6, 10, and 20%). This procedure was performed once in this study. The synthetic urinalysis standard Surine (Dyna-Tek Industries, USA) was also analyzed and used in this study as a control. We have found the Raman spectrum of Surine to be similar to that of urine from healthy volunteers[10] stable over long periods of storage.[12] Raman spectra of Surine were collected at the time of collecting spectra for the hematuria samples described above. The average Raman spectrum of Surine was used as a reference point in the statistical analyses described later.

Raman Spectroscopy

Raman spectroscopy data were acquired using a Peak Seeker dispersive Raman spectrometer (Agiltron, USA). Urine specimens were analyzed as bulk liquid stored in 2 mL flat bottom clear borosilicate glass vials (Thermo Fisher Scientific, no. 03-391-16). The thickness of the vial wall was measured to be 0.78 mm with a digital caliper. Raman scanning was performed using the spectrometer manufacturer's liquid sample vial holder apparatus, where the laser was positioned in contact with the outer edge of the sample vial. Raman scans were acquired at 785 nm, 100 mW laser intensity, 0.2 mm laser spot size, 0.22 numerical aperture, 8 cm^{-1} spectral resolution (manufacturer default), 15 s exposure time, and with a 15 s delay between scans. Spectra were acquired over a 200–2000 cm^{-1} range, and a dark scan was collected for every sample. Spectral data were obtained and dark scans subtracted using RSIQ software (Agiltron), and resulting spectral files contained Raman intensity data every 1 cm^{-1}. Ten independent Raman scans were obtained per sample analyzed, where for each scan, the sample vial was removed, mixed (by vial inversion), and replaced in the sample vial holder.

Raman Spectra Processing and Baselining

All spectral processing and statistical methods were performed in Matlab R2018a and made use of the Rametrix Lite[13] and Pro[9] Toolboxes (available through GitHub). Acquired Raman spectra were first averaged (among replicate scans) and truncated between Raman shifts of 600–1800 cm^{-1}. Next, the scans were baselined, vector normalized, and wavenumber corrected based on urea (aligned to 1002 cm^{-1}). The recently developed ISREA method[22] was used for baselining, as was the established Goldindec algorithm.[21] These different baselining algorithms were applied separately to the same dataset to assess the impact each would have on the statistical analysis. The Goldindec algorithm was used with the following options: polynomial order of three, estimated peak ratio of 0.5, and smoothing window size of five. Iterative smoothing splines with root error adjustment involves the placement of baselining knots or "nodes". These are Raman shifts that anchor the cubic spline baseline along the spectral data. Multiple sets of nodes were tested to observe the effect changing baselining strategies had on data output from the analysis and modeling. The first node set (called the "ISREA node set 1") was developed based on the objective of selecting spectral regions with low signal and variability throughout the dataset. The ISREA node set 2 was constructed to subtract the Raman signal of Surine, the urinalysis control. Finally, the ISREA node set 3 was a control strategy that included 13 evenly spaced nodes from Raman shifts 600 to 1800 cm^{-1}. These nodes are given in Table S1 (Supplemental Material). Statistical analysis was performed given spectral baselining with each set of ISREA nodes, as well as with the Goldindec algorithm.

Analysis of Variance (ANOVA) and Pairwise Comparison Tests

Statistical comparisons among spectra were performed by first calculating the TPD of each urine spectrum relative to the average spectrum of the urinalysis control Surine, as described previously.[10,11,25] With these data, ANOVA and pairwise comparisons were performed, using Tukey's honestly significant difference (HSD) method. ANOVA was used to determine if the differences in Raman spectra between those specimens with added blood and those without were statistically significant. Further, the pairwise comparisons were used to establish if the data provided significant differences between different amounts of blood. The primary determination between the samples was to differentiate between macrohematuria, microhematuria, and no blood (i.e., normal urine). Then, differences among the amounts of blood in the microhematuria samples were determined by pairwise tests between each combination of comparisons (0% versus 0.25%, 0% versus 0.5%, 0.25% versus 1%, etc.) to show the significance or lack thereof. Statistical significance was defined as $p < 0.05$ in all cases.

Principal Component Analysis and Discriminate Analysis of Principal Component Models

Principal component analysis was performed to reduce the complex data of the spectra, identify outlier spectra, and identify the Raman shifts with strong contributions (i.e.,

dominant molecules/bond energies). The selected PCs were then used in DAPC, and several models were built for each dataset, where the number of PCs included was varied. Specifically, DAPC models accommodating between two and 35 PCs were constructed for each dataset. These PCs represented between approximately 65% and 99.95% of the dataset variance, respectively. All models were then validated by external LOOCV as described below.

Partial Least Squares Regression

Partial least squares regression provides a measure of correlation between complex data inputs and a quantitative output. Here, PCs of processed spectra served as inputs and the sample percent blood (v/v%) served as the output. Calculations were performed in Matlab, and the output included the PLS response (training data), the PLS prediction (testing data), the percent variance explained, and the estimated mean-squared prediction error for the dataset. Like DAPC models, the PLSR procedure was also subjected to external LOOCV (discussed below) to assess predictive capabilities given spectra not used to build the model. Goodness of fit results for training and testing data were returned as coefficient of determination (R^2) values.

External Leave-One-Out Cross-Validation

External LOOCV was performed for PCA/DAPC models with the Rametrix Pro Toolbox[9] and with custom scripts for PLSR. Discriminate analysis of principal component models built with different numbers of PCs was assessed individually. Predictions were tabulated at the end of the routine to calculate metrics of overall prediction accuracy, sensitivity, specificity, PPV, and NPV as described previously.[12] The external LOOCV was also applied to PLSR predictions. Here, one sample was systematically left-out of the PLSR model building and was used as the testing dataset. The procedure was performed over the entire dataset, and the coefficient of determination (R^2) was calculated between all PLSR-predicted and actual percent blood values for every sample.

Results

Raman Spectra and Baselining Methods

Raw Raman spectra were processed by Raman shift truncation (600–1800 cm^{-1}), baselining, and vector normalization. The Goldindec and ISREA baselining algorithms were applied to all spectra, and three ISREA node sets were used (see Materials and Methods; Table S1, Supplemental Material). A representative (chosen randomly) averaged and truncated urine spectrum is shown in Fig. 1a and b. Baseline fitting with the Goldindec algorithm and ISREA method with node set 1 is shown in Fig. 1a. The resulting vector normalized (i.e., transformed) spectra are shown in Fig. 1b. The Goldindec algorithm leveled the spectrum endpoints as well as the lowest mid points. The ISREA algorithm with node set 1 resulted in significantly different normalized signal intensities (compared to Goldindec) in the Raman shift regions of 1050–1250 cm^{-1} and 1590–1750 cm^{-1} Raman shifts (Fig. 1b).

The influence of added blood on the urinalysis control Surine spectrum is shown in Fig. 1c, where representative spectra with 0, 2, and 6% (v/v) blood were added. In Fig. 1c, spectra were baselined with the Goldindec algorithm but not vector normalized, and regions of observed Raman intensity changes were labeled one through five. Heme and red blood cell Raman bands have been identified in the literature[20,26] at (among others) Raman shifts: 669, 750, 752, 999, 1122, 1210, 1444, 1542–3, 1579, and 1614–7 cm^{-1}. As evident in Fig. 1c, our analysis of dilute blood in urine did not return strong intensities at these Raman shifts, except for 1614–7 cm^{-1}. Region 2 (~1002 cm^{-1}) of Fig. 1c most closely correlates with urea in urine.[10] With added blood volume, this signal (1002 cm^{-1}) was diluted significantly. With this, we also observed decreases in signal intensity at the other labeled regions of the spectra (Fig. 1c) but to different degrees. No large signal increases from added blood were evident over the 600–1800 cm^{-1} Raman shift range analyzed (Fig. 1c). However, the ratios of the Raman intensities in regions one to five (and others not identified here) changed differentially with added blood. For example, in Fig. 1c, the ratio of the signals between regions five and two was ~42%, with 0% blood added. This ratio increased to ~59% with 6% blood added. We sought to build chemometric models in this research that could identify these relationships and relate them to hematuria levels qualitatively (DAPC) and quantitatively (PLSR).

We also examined whether the choice of baselining method would influence the accuracy of these DAPC and PLSR models. The analysis of Surine shown in Fig. 1c was repeated given ISREA baselining, and results are shown in Supplemental Figs. S2–4. Spectra given 0, 2, and 6% blood are shown in Supplemental Figs. S2 through S4. These illustrate that the change in ratios, described for Fig. 1c, is baseline dependent. Further, the total range of Raman signal at each Raman shift is given in Fig. 1d for Goldindec baselining and in Supplemental Figs. S2 through S4 for ISREA baselining.

Finally, we have included Goldindec baselined scans of Surine and an empty vial together in Supplemental Fig. S5. This highlights both the real Raman signal being acquired from Surine, particularly the strong urea signal (1002 cm^{-1}), and the background fluorescence that was unable to be subtracted through dark scan subtraction and baselining, particularly between 600–950 cm^{-1}. In addition, most of the data rich portion of the spectra belonging to Surine (and urine) occurs around 1120–1200 cm^{-1}, which can be associated with carbohydrates, collagen, and carotenoids,[26] and between 1300–1800 cm^{-1}. In particular, the 1590–1750 cm^{-1} region shows significant differences between Surine and the empty vial control (Supplemental Fig. S5). This region is dominated by protein assignments, namely related to aromatic amino acids,[26] and those identified

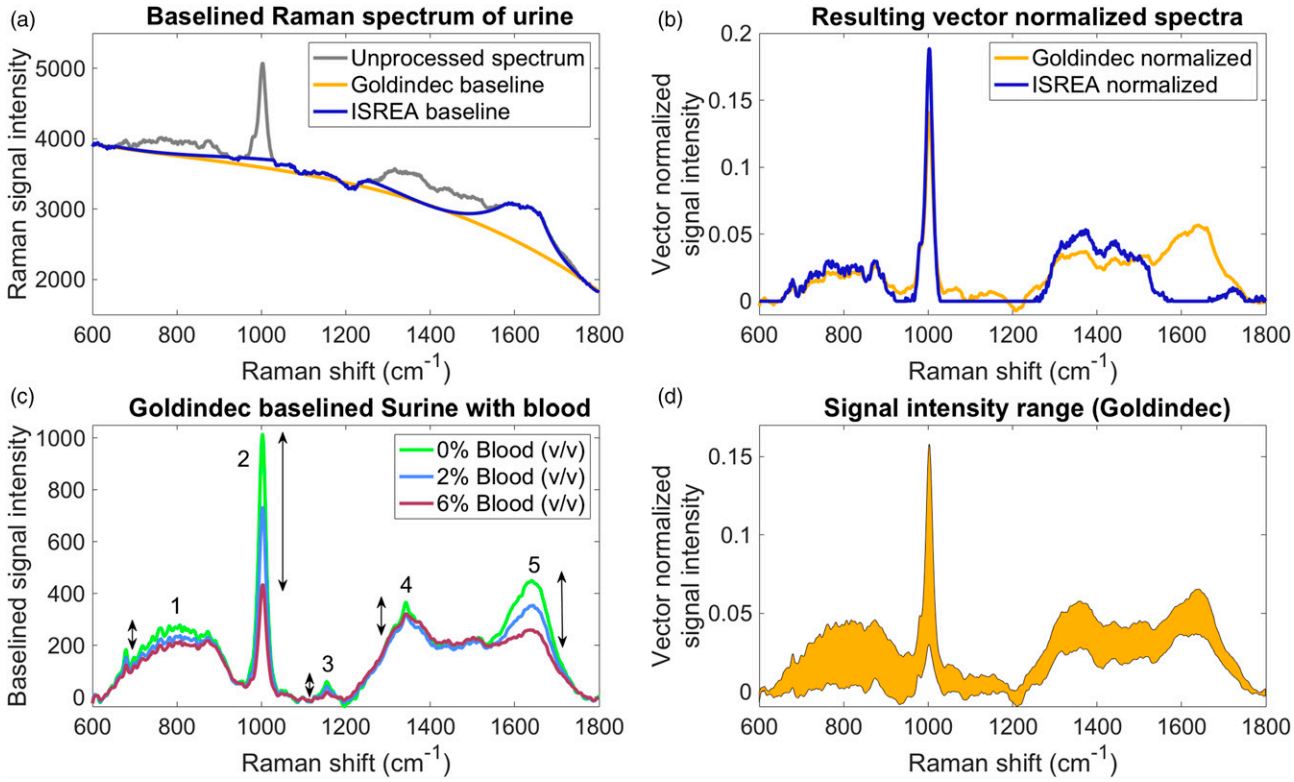

Figure 1. Raman spectra of urine and Surine with hematuria. (a) An unprocessed urine spectrum with Goldindec and ISREA (node set 1) baselining, (b) Resulting vector normalized transformed spectra, (c) Goldindec baselined spectra of Surine with added blood (0, 2, and 6% v/v) and highlighted regions (1–5) of observed spectral intensity changes, (d) The range of signal intensities (shaded region) at each Raman shift between 600–1800 cm^{-1} for urine samples, all levels of blood (0–20% v/v), and Goldindec spectral baselining.

for blood mentioned earlier. Next, we sought to determine whether chemometric models could be used to predict the presence and level of hematuria in urine.

We first applied the Goldindec algorithm to all analyses due to our prior success with this algorithm and the popularity of polynomial-based baselining algorithms.[27] This was done in the next section, Analysis of All Hematuria Samples, which included the no blood (0% v/v), microhematuria (0.25–1% v/v), and macrohematuria (2–20% v/v) samples. The ISREA method was implemented to further resolve the no blood and microhematuria samples in the following Analysis of No Blood and Microhematuria section of the Results.

Analysis of All Hematuria Samples

Statistical Analyses. Total principal component distance data[10] were generated from processed spectra baselined with the Goldindec algorithm. First, ANOVA was performed these TPD data given sample classifications of macrohematuria, microhematuria, and no blood. Statistical significance ($p < 0.05$) was observed for differences among these classes of spectra. Next, statistical significance was also observed when the analysis was performed based on the volume of blood added to the urine samples (i.e., 0%, 0.25%, 0.5%, 1%, 2%, 6%, 10%, and 20% v/v).

From here, pairwise comparisons were performed. For comparison of microhematuria, macrohematuria, and no blood classifications, all pairwise comparisons returned statistical significance (Supplemental Table S2). For the blood volume classifications, 16/28 (57%) of the comparisons showed statistical significance (Supplemental Table S3). This number suggested that distinguishing among blood volume classifications (e.g., 0%, 0.25%, and 1%) in further modeling may be limited. In addition, the number of statistically significant pairwise comparisons was likely limited by the population size of this initial proof of concept study.

Classifications with PCA and DAPC

Principal component analysis and DAPC were performed with Rametrix LITE on the spectral data using both classifications mentioned above. The PC loading data for this analysis are provided in the Supplemental Material. The DAPC results for both classifications are given as cluster plots in Fig. 2. Here, DAPC results were generated using 19 PCs (representing 99.4% of the dataset variance) of the spectral data. With 19 PCs, 19 canonical dimensions were created by the DAPC analysis. The first three dimensions are shown in Fig. 2a and two in Fig. 2b to demonstrate clustering, where clusters are indicative of similar processed Raman spectra. Cluster separation

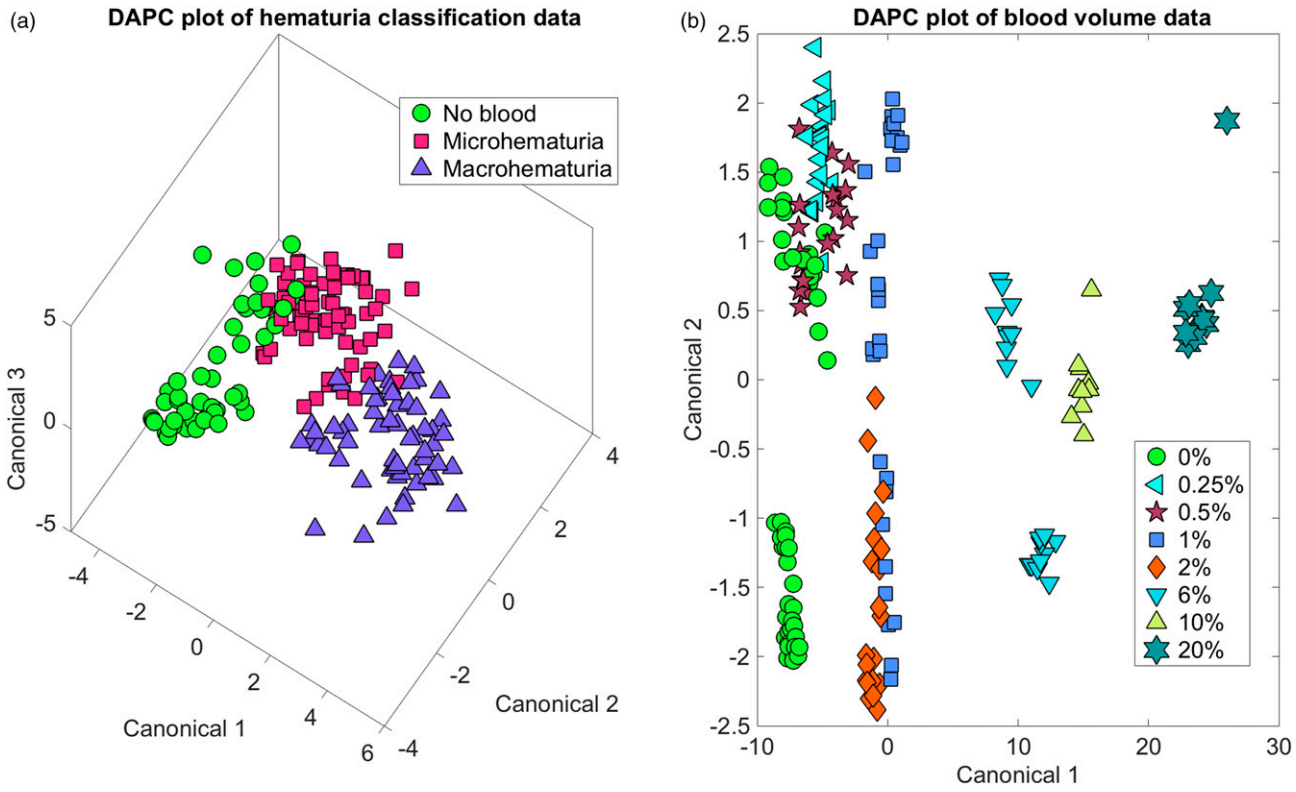

Figure 2. DAPC plots of hematuria classifications. (a) Macrohematuria, microhematuria, and no blood and (b) percent blood (v/v) of each urine sample. DAPC was performed with 19 PCs, representing 99.4% of spectral dataset variance.

Table I. DAPC External LOOCV Results for Hematuria Status Classification.

Classification	Accuracy (%)	Sensitivity (%)	Specificity (%)	PPV (%)	NPV (%)
DAPC model built with 19 PCs (99.4% of dataset variance)					
No Blood	94	80	100	100	93
Microhematuria	91	97	86	82	98
Macrohematuria	96	93	97	93	97
DAPC model built with six PCs (98.7% of dataset variance)					
No Blood	90	78	95	87	92
Microhematuria	82	97	72	69	98
Macrohematuria	90	93	88	80	96

with some overlap was achieved between macrohematuria, microhematuria, and no blood in Fig. 2a, with the microhematuria cluster appearing between those of macrohematuria and no blood along the first canonical. We were unsure why the no blood group separated along Canonical 2 in Fig. 2a and b, but it is noted that the group was not separated along Canonical 1, which showed more importance for separating clusters in both cases. For the analysis by blood volume, in Fig. 2b, the samples clustered from left to right along canonical one according to increasing blood volume concentrations. The DAPC model had no knowledge of the blood concentrations during model building; it was only informed that the groups were different. The arrangement according to increasing blood concentration from left to right along Canonical 1 validates blood concentration was responsible for the separation among groups, rather than random or non-specific signal/fluorescence.

Next, Rametrix PRO was used to perform external LOOCV on the DAPC model shown in Fig. 2a and determine prediction metrics for unknown urine samples. Results are shown in Table I for each classification. Prediction accuracy exceeded 90% for classifying an unknown urine sample as "macrohematuria," "microhematuria," or "no blood" (Table I). However, some metrics (e.g., sensitivity for classifying a sample as no blood) failed to reach 90%. The analysis was repeated for DAPC models built with fewer PCs. First, six PCs

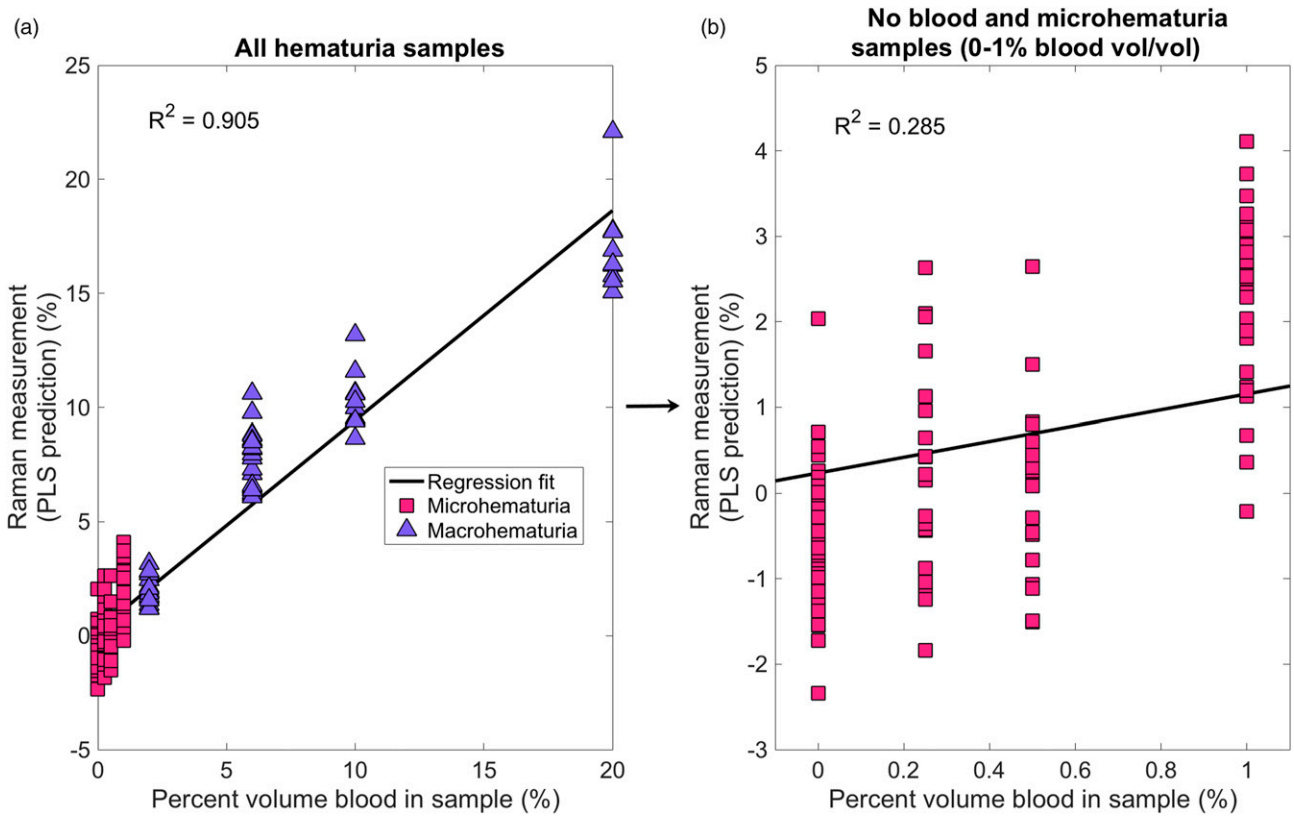

Figure 3. Raman measurement PLSR external LOOCV predictions versus actual percent blood in urine samples (v/v). (a) Over all hematuria samples and (b) for no blood and microhematuria (0–1% blood volume).

were chosen (representing 98.7% of the dataset variance). These results are also shown in Table I. Overall prediction accuracies for samples classified as no blood and macrohematuria exceeded 90%. This was about 82% for microhematuria. Finally, for a DAPC model built with three PCs (representing 94.7% of the dataset variance), the overall prediction accuracies were 78%, 74%, and 83% for no blood, microhematuria, and macrohematuria, respectively, and they were similar for a model built with two PCs. However, given the three possible classifications for an unknown urine sample (i.e., no blood, microhematuria, or macrohematuria), these models far exceeded the random chance correct prediction rate of 33%.

Partial Least Squares Regression

To return a quantitative value of hematuria based on the Raman spectrum for a sample, PLSR with external LOOCV was implemented. Results are shown in Fig. 3, with the line of regression fit showing the correlation between the Raman measurement predicted values (from PLSR and external LOOCV) and the actual blood percent volume in urine samples. The coefficient of determination (R^2) was greater than 0.9 when considering all samples (i.e., no blood, microhematuria, and macrohematuria), as shown in Fig. 3a. However, the correlation for no blood and microhematuria samples only (i.e., 0–1% blood v/v) was much less (R^2 = 0.285), as shown in Fig. 3b. This R^2 value suggests this PLSR model performs better for macrohematuria than for blood volumes below 1%. The microhematuria region is important for accurate measurements by Raman spectroscopy as blood may not be visible by visual inspection at these levels. Thus, additional data analysis techniques were explored for better quantifying Raman spectra of no blood and microhematuria samples.

Analysis of No Blood and Microhematuria Samples

To improve the determination of percent blood in urine, in the 0–1% v/v range, by Raman measurements, we employed ISREA baselining with node sets one through three in addition to the Goldindec algorithm. The baseline fits and resulting vector normalized spectra for all baselining algorithms used are shown in Fig. 1 and Fig. S1 (Supplemental Material). The overall goal of the following approach was to improve the correlation between Raman measurements and actual percent blood in urine specimens (R^2 = 0.285). As apparent in Fig. 1 and S1 (Supplemental Material), the choice of node set for ISREA can transform Raman spectra significantly. Regions of the spectra can be emphasized/minimized, and we sought to determine whether this could be used to resolve the no blood and microhematuria region of the dataset.

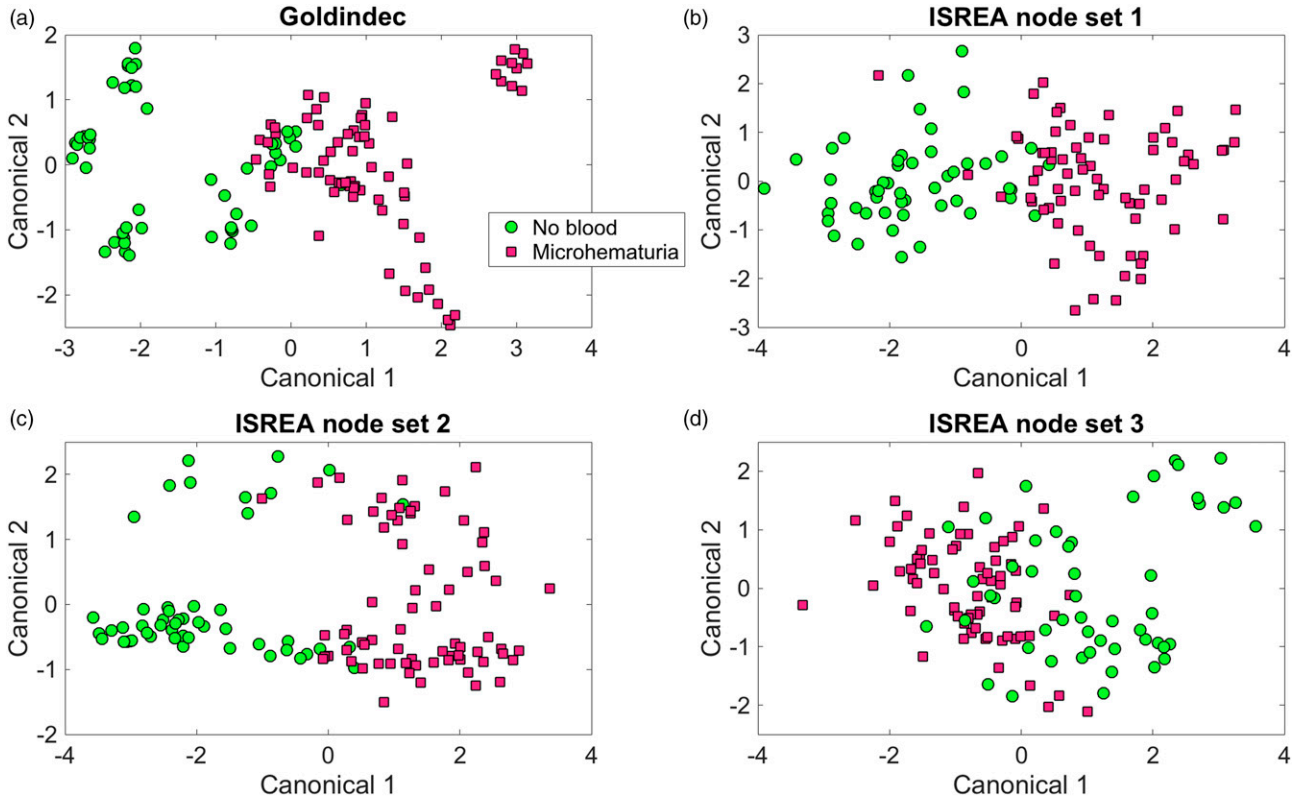

Figure 4. DAPC plots to distinguish between no blood and microhematuria given different spectral baselining. (a) Goldindec algorithm, (b) ISREA node set 1, (c) ISREA node set 2, and (d) ISREA node set 3.

Table II. DAPC External LOOCV Results Identification of Microhematuria.

Baselining method	PCs[a]	Accuracy (%)	Sensitivity (%)	Specificity (%)	PPV (%)	NPV (%)
Goldindec	8	91	100	78	86	100
ISREA node set 1	12	94	100	86	91	100
ISREA node set 2	9	90	76	100	100	85
ISREA node set 3	20	86	97	70	82	95

[a]The number of PCs included represented 99% of the dataset variance.

Statistical Analyses

The ANOVA results for the comparison of no blood versus microhematuria samples (i.e., with macrohematuria samples excluded) showed statistical significance ($p < 0.001$) for each ISREA node set. Pairwise comparisons, however, differed given the different baselining methods, and results are given in Supplemental Table S4. In summary, the Goldindec and ISREA node set two algorithms each returned 1/6 (<17%) pairwise comparisons with statistical significance ($p < 0.05$). Iterative smoothing splines with root error adjustment with node set 3 did not return any with statistical significance, and ISREA with node set 1 returned 5/6 (>83%) with statistical significance. This provided strong evidence that the choice of baselining method could influence the detection of microhematuria. We have interpreted the results to suggest that ISREA node set 1 removes or reduces spectral data which otherwise conflates other data points. While all baseline methods led to statistical separation between no blood and microhematuria samples, only ISREA node set 1 showed the ability to differentiate between different blood volumes at the microhematuria level.

Table III. PLSR external LOOCV correlations (R^2) for raman measurements and microhematuria percent blood volumes (0–1%).

Baselining method	R^2
Goldindec	0.876
ISREA node set 1	0.920
ISREA node set 2	0.691
ISREA node set 3	0.547

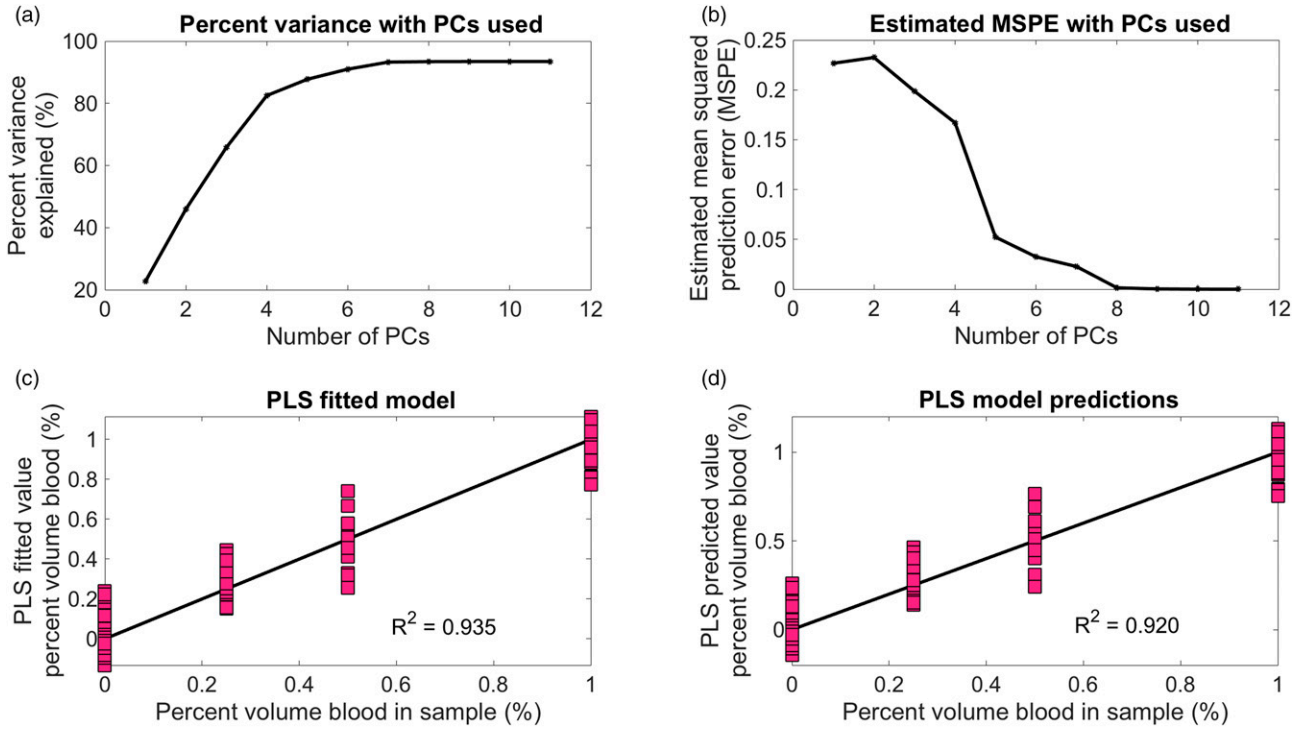

Figure 5. PLSR modeling results for no blood and microhematuria. (a) Percent variance as a function of PCs used, (b) Estimated mean squared prediction error (MSPE) as a function of PCs used, (c) PLSR model training, and (d) PLSR external LOOCV model testing results.

Classifications with PCA and DAPC

Again, PCA and DAPC models were built but only included the no blood and microhematuria samples. Discriminate analysis of principal component clustering results are shown in Fig. 4 for the Goldindec and all ISREA baselining methods. Differences in cluster separations were apparent, especially with ISREA node set 3, which showed considerable overlap. Each DAPC model in Fig. 4 was built with the number of PCs required to represent 99% of the dataset variance. Next, external LOOCV was applied to determine prediction metrics for distinguishing whether an unknown urine sample belonged to the no blood or microhematuria classification. These results are shown in Table II. Both the Goldindec algorithm and ISREA node set 1 exceeded 90% prediction accuracy and showed 100% sensitivity and NPV. The ISREA node set 1 showed improved specificity and PPV metrics. The ISREA node set 2 method showed 90% overall accuracy with 100% specificity, and ISREA node set 3 showed the least accurate predictions.

Partial Least Squares Regression

The PLSR correlations (R^2) between Raman measurements, no blood, and microhematuria percent blood concentrations are given in Table III. These were generated from external LOOCV of the PLSR model. Of note the Goldindec algorithm improved from an R^2 of 0.285 to 0.876 when including all hematuria samples (Fig. 3) or only no blood and microhematuria (Table III). This demonstrates how an initial DAPC classification of hematuria (Fig. 2a) may be useful in determining which PLSR model to apply. The ISREA node set 1 outperformed the Goldindec algorithm slightly in Table III. The specific PLSR results for ISREA node set 1 are shown in Fig. 5. The effect from number of PLS components used is shown in Fig. 5a. For the purposes of this analysis, 11 components were chosen, as this was found to maximize the percent variance explained as well as improve our prediction capabilities. The PLSR model training is shown in Fig 5c (R^2 = 0.935), and the PLSR model testing results with external LOOCV is given in Fig. 5d (R^2 = 0.920). While the ISREA node set 1 generated the highest R^2 value among the baselining methods tested, it is clear that the choice of node set weighs heavily on the predictive capability of a PLSR model given Raman spectra inputs.

Discussion

The use of Raman spectroscopy for detection and quantification of hematuria with high accuracy and low cost has important implications, including near-real time testing at points of patient care, low cost/test, and accuracy to guide clinical decisions. This proof of concept study demonstrated the capacity to detect and quantify macro- and microhematuria in dilute urine with Raman spectroscopy and chemometric analyses. We focused here on

the impact of the predictive capabilities of PCA–DAPC (qualitative) and PLSR (quantitative) given different spectral baselining methods, and how statistical tests (ANOVA and pairwise comparisons of TPD data) can help inform predictive capabilities of these models. The impact of baselining algorithm, on the predictive capabilities of a DAPC or PLSR model, was demonstrated. Choosing a reliable, application agnostic method of baselining, such as Goldindec, has its advantages, but choosing a method that has more customization options, such as ISREA, can improve the outcome.

The Agiltron Peak Seeker Raman spectrometer used in this study is relatively low-cost, low-profile, and portable, and the consumable clear borosilicate glass sample vials are also low-cost and are a readily available standard item. It is noted, however, that, in our experience, the choice of vial for liquid Raman analysis can be critical. We have seen that glass types can contribute fluorescence and Raman intensities to the background signal. The specific vials used in this research (Thermo Fisher Scientific, no. 03-391-16) minimized these effects in our spectra (Supplemental Fig. S5); however, users should be aware of the effects of glass chemistry, glass wall thickness, and laser probe positioning when obtaining Raman spectra of liquid samples, including urine. Approaches, such as comparison to standards (like Surine in this research) can help mitigate these effects, and we have seen that ISREA baselining is effective at removing effects of residual fluorescence from spectra.[22]

Conclusion

In summary, we were able to distinguish between macro- and microhematuria with 96% overall accuracy and found that determination of microhematuria was inaccurate for micro-levels of blood ($R^2 = 0.28$). By refining computational modeling to only microhematuria levels of blood (<1% v/v) and incorporating ISREA baselining, a high level of correlation ($R^2 = 0.92$) was achieved, leading to high predictive accuracy. Overall, this study suggests that Raman spectroscopy, baselining, PCA, DAPC, ANOVA, pairwise comparisons, PLSR, and external LOOCV can be utilized to perform screening or rapid testing for the presence of blood in urine, as well as identify the level of blood with high accuracy. However, we acknowledge that this study only provides a first proof of concept for the technology. Only a single blood draw and urine specimen were used in this study. It is likely that several large-scale studies will be required to detect hematuria from diverse sets of blood/urine samples, especially for those associated with kidney, bladder, urinary tract, metabolic diseases, and/or blood disorders. Further, the Raman shifts utilized by our chemometric models were not based on documented bands for heme groups and red blood cells in the Raman literature. However, with a large enough knowledge base, this type of Raman-based rapid screening technology could be automated, enabling early hematuria detection while screening urine for other diseases simultaneously.

Acknowledgments

We also acknowledge contributions of Amr Sayed Issa in the revision of this manuscript.

Author contributions

The study was designed by JLR. Experiments and measurements were performed by WC. Data analysis was performed by WC and RSS. All authors contributed to the manuscript.

Declaration of Conflicting Interests

RSS and JLR co-founded DialySensors, Inc. with intention to commercialize technologies described in this manuscript. Rametrix has been trademarked by DialySensors, Inc. (Blacksburg, VA)..

Funding

The author(s) disclosed receipt of the following financial support for the research, authorship, and/or publication of this article: This research was funded in part the Center for Innovative Technology (award CP15-015-LS), the Virginia Tech Foundation, and HATCH (project VA-160057). The funding agencies had no role in the research or manuscript preparation.

Supplemental Material

The supplemental material mentioned in the text, consisting of additional figures, tables, and raw data, is available in the online version of the journal.

ORCID iDs

John L. Robertson https://orcid.org/0000-0003-4361-999X
Ryan S. Senger https://orcid.org/0000-0002-2450-6693

References

1. B.L. Khoo, C. Bouquerel, P. Durai, et al. "Detection of Clinical Mesenchymal Cancer Cells from Bladder Wash Urine for Real-Time Detection and Prognosis". Cancers. 2019. 11(9): 1274. doi:10.3390/cancers11091274.
2. M. Nielsen, A. Qaseem. "Hematuria as a Marker of Occult Urinary Tract Cancer: Advice for High-Value Care from the American College of Physicians". Ann. Intern. Med. 2016. 164(7): 488-497. doi:10.7326/M15-1496.
3. W.R. Premasiri, R.H. Clarke, M.E. Womble. "Urine Analysis by Laser Raman Spectroscopy". Lasers Surg. Med. 2001. 28(4): 330-334. doi:10.1002/lsm.1058.
4. V. Kavuru, T. Vu, L. Karageorge, et al. "Dipstick Analysis of Urine Chemistry: Benefits and Limitations of Dry Chemistry-based Assays". Postgrad. Med. 2020. 132(3): 225-233. doi:10.1080/00325481.2019.1679540.
5. R. Ghandour, Y. Freifeld, N. Singla, Y. Lotan. "Evaluation of Hematuria in a Large Public Health Care System". Bladder Cancer Amst. Neth. 2019. 5(2): 119-129. doi:10.3233/BLC-190221.
6. M.O. Saleem, K. Hamawy. "Hematuria". In: StatPearls. Treasure Island, Florida: StatPearls Publishing, 2021. https://www.ncbi.nlm.nih.gov/books/NBK534213/.

7. F. Liedberg, U. Gerdtham, K. Gralén, et al. "Fast-Track Access to Urologic Care for Patients with Macroscopic Haematuria is Efficient and Cost-Effective: Results from a Prospective Intervention Study". Br. J. Cancer. 2016. 115(7): 770-775. doi:10.1038/bjc.2016.265.
8. J.L. Whiteside, H.T.H. Yuen. "Asymptomatic Microscopic Hematuria in Women". Curr. Opin. Obstet. Gynecol. 2019. 31(6): 471-476. doi:10.1097/GCO.0000000000000573.
9. R.S. Senger, J.L. Robertson. "The Rametrix PRO Toolbox v1.0 for Matlab". PeerJ. 2020. 8: e8179. doi:10.7717/peerj.8179.
10. R.S. Senger, V. Kavuru, M. Sullivan, et al. "Spectral Characteristics of Urine Specimens from Healthy Human Volunteers Analyzed Using Raman Chemometric Urinalysis (Rametrix)". PLoS One. 2019. 14(9): e0222115. doi:10.1371/journal.pone.0222115.
11. R.S. Senger, M. Sullivan, A. Gouldin, et al. "Spectral Characteristics of Urine from Patients with End-Stage Kidney Disease Analyzed Using Raman Chemometric Urinalysis (Rametrix)". PLoS One. 2020. 15(1): e0227281. doi:10.1371/journal.pone.0227281.
12. H.M. Huttanus, T. Vu, G. Guruli, et al. "Raman Chemometric Urinalysis (Rametrix) as a Screen for Bladder Cancer". PLoS One. 2020. 15(8): e0237070. doi:10.1371/journal.pone.0237070.
13. A.K. Fisher, W.F. Carswell, A.I.M. Athamneh, et al. "The Rametrix LITE Toolbox v1.0 for Matlab". J. Raman Spectrosc. 2018. 49(5): 885-896. doi:10.1002/jrs.5348.
14. I. Tanniche, E. Collakova, C. Denbow, R.S. Senger. "Characterizing Glucose, Illumination, and Nitrogen-Deprivation Phenotypes of *Synechocystis* PCC6803 with Raman Spectroscopy". PeerJ. 2020. 8: e8585. doi:10.7717/peerj.8585.
15. L.P. Moreira, L. Silveira, A.G. da Silva, et al. "Raman Spectroscopy Applied to Identify Metabolites in Urine of Physically Active Subjects". J. Photochem. Photobiol. B. 2017. 176: 92-99. doi:10.1016/j.jphotobiol.2017.09.019.
16. O. Žukovskaja, O. Ryabchykov, M. Strassburger, et al. "Towards Raman Spectroscopy of Urine as Screening Tool". J. Biophotonics. 2020. 13(1): e201900143. doi:10.1002/jbio.201900143.
17. D.R. Parachalil, J. McIntyre, H.J. Byrne. "Potential of Raman Spectroscopy for the Analysis of Plasma/Serum in the Liquid State: Recent Advances". Anal. Bioanal. Chem. 2020. 412(9): 1993-2007. doi:10.1007/s00216-019-02349-1.
18. D. Qi, A.J. Berger. "Quantitative Concentration Measurements of Creatinine Dissolved in Water and Urine using Raman Spectroscopy and a Liquid Core Optical Fiber". J. Biomed. Opt. 2005. 10(3): 031115. doi:10.1117/1.1917842.
19. W. Zhu, B.-Y. Wen, L.-J. Jie, et al. "Rapid and Low-Cost Quantitative Detection of Creatinine in Human Urine with a Portable Raman Spectrometer". Biosens. Bioelectron. 2020. 154: 112067. doi:10.1016/j.bios.2020.112067.
20. N. Huang, M. Short, J. Zhao, et al. "Full Range Characterization of the Raman Spectra of Organs in a Murine Model". Opt. Express. 2011. 19(23): 22892-22909. doi:10.1364/OE.19.022892.
21. J. Liu, J. Sun, X. Huang, et al. "Goldindec: A Novel Algorithm for Raman Spectrum Baseline Correction". Appl. Spectrosc. 2015. 69(7): 834-842. doi:10.1366/14-07798.
22. Y. Xu, P. Du, R. Senger, et al. "ISREA: An Efficient Peak-Preserving Baseline Correction Algorithm for Raman Spectra". Appl. Spectrosc. 2021. 75(1): 34-45. doi:10.1177/0003702820955245.
23. M.L. Olson, J. Johnson, W.F. Carswell, et al. "Characterization of an Evolved Carotenoids Hyper-Producer of *Saccharomyces cerevisiae* Through Bioreactor Parameter Optimization and Raman Spectroscopy". J. Ind. Microbiol. Biotechnol. 2016. 43(10): 1355-1363. doi:10.1007/s10295-016-1808-9.
24. S.H. Chung, K.S. Park. "A Study on the Factor Number Determination Methods in the Partial Least Squares Model for the Urinalysis Using Raman Spectroscopy". In: The 26th Annual International Conference of the IEEE Engineering in Medicine and Biology Society. San Francisco, California: September 1-5, 2004. Pp. 490-493. doi:10.1109/IEMBS.2004.1403201.
25. S. Li, J.O. Nyagilo, D.P. Dave, J. Gao. "Models and Methods for Quantitative Analysis of Surface-Enhanced Raman Spectra". IEEE J. Biomed. Health Inform. 2014. 18(2): 525-536. doi:10.1109/JBHI.2013.2281947.
26. Z. Movasaghi, S. Rehman, D.I.U. Rehman. "Raman Spectroscopy of Biological Tissues". Appl. Spectrosc. Rev. 2007. 42(5): 493-541. doi:10.1080/05704920701551530.
27. R.S. Senger, D. Scherr. "Resolving Complex Phenotypes with Raman Spectroscopy and Chemometrics". Curr. Opin. Biotechnol. 2020. 66: 277-282. doi:10.1016/j.copbio.2020.09.007.